PLIF OF OH IN HIGH PRESSURE CRYOGENIC LOx/GH_2 JET FLAMES

G. Singla, P. Scouflaire, C. Rolon, S. Candel
CNRS - Laboratoire EM2C, Grande Voie des Vignes, 92295 Chatenay-Malabry, France

This article deals with the application of OH planar laser induced fluorescence (PLIF) to the study of high pressure cryogenic flames. High pressure conditions require a careful choice of the excitation wavelength based on a detailed analysis of the absorption coefficient dependence with respect to pressure and temperature. PLIF is used to examine jet flames formed by a single coaxial injector fed by liquid oxygen and gaseous hydrogen (LOx/GH_2) in subcritical and transcritical regimes. In the last case, the liquid oxygen temperature is below its critical value while the pressure is above critical. Such transcritical conditions prevail in many high performance devices like liquid propellant rocket engines. A detailed understanding of this type of combustion is necessary to the development of improved and more reliable propulsion systems. PLIF provides images which may be considered to represent instantaneous distribution of OH radicals and may be used to infer the structure and position of the flame.

Experiments are carried out on the Mascotte cryogenic test bench of Onera. It is shown that OH PLIF provides good quality images up to 6.3 MPa. The resulting data can be used to examine the flame structure in the nearfield of the injector. It is known from a previous analysis of the flame holding mechanism that the low speed wake established just behind the oxygen injector lip and generated by the two propellants must be thicker than the flame edge thickness to ensure a stable anchoring. PLIF images indicate that the flame thickness is of the order of the wake transverse size. When the thickness exceeds this transverse dimension it is found that the flame becomes sensitive to the high speed hydrogen stream.

The dependence of the fluorescence signal with respect to pressure, temperature and species mole fraction is examined in detail in [1]. A description of the experimental set-up and optical diagnostics is given in the next section. The second section includes data from laser induced fluorescence and images obtained from direct detection of spontaneous light emission from OH^* radicals. The last section contains a discussion of the cryogenic flame holding mechanism based on close-up views of the flame edge behind the oxygen lip.

1. Cryogenic combustion facility

High pressure experiments are carried out on a cryogenic model scale combustor designated as “Mascotte”. This facility operated by Onera and represented schematically in Fig. 1 can be used to study LOx/H_2 or LOx/CH_4 combustion (version V04). The most notable changes with respect to the previous versions of Mascotte concern the fuel feed line, which was modified to allow injection of either hydrogen or methane. The heat exchanger, placed on the feed system, is powerful enough to (1) Liquify the methane stream at a maximum mass

flow rate $\dot{m}_{CH_4} = 250$ g s^{-1} (2) Cool down the hydrogen stream from room temperature to 100 K at a maximum flow rate $\dot{m}_{H_2} = 100$ g s^{-1}. In most experiments the hydrogen is injected at 288 K. It is thus possible to (1) Investigate combustion conditions in which liquid methane is injected together with liquid oxygen [2] (2) Study effects of reducing the hydrogen temperature injection [3]. The maximum liquid oxygen flow rate is $\dot{m}_{LOx} = 200$ g s^{-1} but most studies are carried out with mass flow rates $\dot{m}_{LOx}$ ranging from 40 to 100 g s^{-1}. The flame spreads in a combustion chamber capable of withstanding pressures up to 10 MPa. This unit has a square cross section of 50×50 mm^2. A visualization module equipped with 75 mm long windows on its four sides can be placed at any point along the chamber, allowing exploration of chamber sections located at various distances from the injection plane (the total chamber length is 425 mm). The window internal faces are cooled by a gaseous helium film. The quartz windows are transparent to near UV radiation and they can be used to transmit a longitudinal light sheet for laser imaging. In the present experiments, the visualization module was located against the injection plane, providing a full view of the initial flame. Interchangeable converging-diverging nozzles made of graphite define the operating pressure.

2. Diagnostics and processing methods

The setup shown in Fig. 1 includes an OH PLIF system, an optical multichannel analyzer for spectroscopic investigations and light emission imaging using an intensified CCD camera.

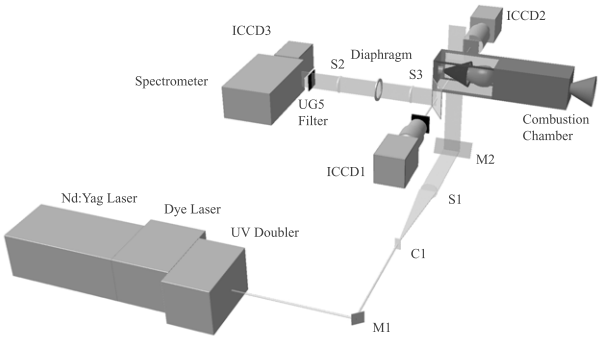

Fig. 1: Schematic representation of the experimental setup.

The laser sheet used to pump the OH radical is generated by a Nd:YAG - pumped frequency doubled dye laser (Continuum Powerlite Precision II, Continuum ND6000, Continuum UVT-2) tuned to the $Q_{11}(9.5)$ transition of the $A^2\Sigma^+ - X^2\Pi$ ($v' = 1$, $v'' = 0$) band. The typical pulse energy in the UV around 284 nm is 42 mJ with a duration of 10 ns. The typical laser bandwidth FWHM is 0.15 cm^{-1}. The UV laser beam was expanded to a diameter of 5 mm. As shown in Fig. 1 a spherical convergent lens ($f_{S1} = 860$ mm, UV 284 nm) associated with a UV grade fused silica cylindrical divergent lens ($f_{C1} = -75.6$ mm) and two mirrors M1 ($\phi = 25$ mm, UV 284 nm), M2 (120×25 mm^2, UV 284 nm) are used to form the incident laser beam into a thin sheet. The telescope setup is employed to expand the beam in one dimension forming a narrow sheet of light which is then focused in the chamber. Sheet dimensions are approximately 41 mm by 500 μm. The gaussian wings of the laser beam are not used to illuminate the region of interest so that the intensity in the sheet is nearly constant. For the laser output and for this light sheet geometry, one obtains power densities of the order of 15 MW cm^{-2}. This is relatively high and one may ask whether this might not lead to saturation. It is not possible to check the signal linearity under the present hot fire conditions but there are many experiments at atmospheric pressures which employ power fluxes reaching 8 MW cm^{-2}. These experiments are considered to lie in the linear range. It is also known that the saturation intensity increases like the square of the pressure [4]. In this reference the problem is discussed and it is indicated that no saturation was observed in experiments at intermediate pressure (3 MPa) and at half of the power used in our case. One may then safely conclude that fluorescence remains in the linear regime and that a margin exists before saturation is reached under the conditions of this experiment.

The fluorescence signal is collected by a Princeton Instruments 5 MHz ICCD camera with a 120 μm resolution (close up on the injector nearfield) at a rate of 10 Hz. The exposure time is fixed at a value of 50 ns. The intensifier is used to gate the fluorescence signal to achieve a higher signal to noise ratio. Light is collected by a UV Nikkor 105 mm/f 4.5 objective. The ICCD camera placed at right angles to the flow direction in the chamber, is fitted with two WG305 filters to block the elastic scattering from the incident beam and the possible Raman signal scattered by the liquid oxygen jet. A 308BP15 band pass filter

with a FWHM of 15 nm and a peak transmission of 25 % at 308 nm is used to transmit fluorescence from the $A - X\,(1,1)$ and $A - X\,(0,0)$ vibrational bands $(306 - 320\,\text{nm})$.

In the spectroscopic mode, fluorescence is collected using two spherical convergent UV grade fused Silica lenses ($f_{S2} = 650\,\text{mm}$, $f_{S3} = 1200\,\text{mm}$) and a diaphragm to limit spherical aberrations. The collected fluorescence signal is guided to the Optical Multichannel Analyzer (Acton Spectra Pro 2500i) fitted with a Princeton Instruments ICCD camera 1024×1024 pixels. The cryogenic flame image is projected on the slit (14 mm) of the OMA and scattered by a 2400 gr/mm grating. The second order of the grating was rejected using a UG5 filter (400 nm short pass filter) placed in front of the entrance slit thus effectively increasing the spectral resolution. With these parameters, fluorescence spectra were recorded in the spectral range between 306 nm and 316 nm with a UV spectral resolution of about 0.01 nm. The exposure time of the ICCD camera running in spectroscopic mode was fixed at a value of 50 ns to ensure detection of the fluorescence from the $A - X\,(1,1)$ and $A - X\,(0,0)$ vibrational bands.

Spontaneous light emission of OH^* radicals is recorded at a rate of 10 Hz with a Princeton Instruments 5 MHz ICCD camera with a resolution of 200 μm. The camera is equipped with a UV Nikkor 105 mm/f 4.5 objective. A UG5 glass filter is used to block radiations above 400 nm and a WG305 glass filter to suppress radiation below 283 nm, while passing 50-70% of the light emitted between 306 and 320 nm where chemiluminescence is observed. The exposure time was fixed at 1 μs to obtain nearly instantaneous images. OH PLIF and spectroscopic measurements are simultaneous while detection of OH^* chemiluminescence is delayed by 1 μs to eliminate any fluorescence signals. Flow velocities in the combustion chamber range from 10 m s^{-1} to 100 m s^{-1} [5]. Under these conditions, with a gate delay of 1 μs, turbulent eddies are slightly deformed by 10 μm to 100 μm but these displacements are below the spatial resolution of the ICCD1 camera. The images provided by each diagnostic can be considered simultaneous.

3. High pressure OH PLIF imaging

High pressure OH fluorescence spectra were recorded and compared with synthesized ones. A spectral analysis carried out in [1] shows that the signal detected on the combustor sideline has the expected features of OH fluorescence. It is then interesting to focus on images recorded by the ICCD camera at high pressure. The intensity level observed can be interpreted as being related and to some extent linearly to the local molar fraction of OH. The hot fire test conditions are given in Table 1. The desired value of the chamber pressure is fixed by the convergent-divergent choked nozzle and by the liquid oxygen and gaseous hydrogen mass flow rates. The chamber pressure value is sensitive to these two parameters, and more specifically to the liquid oxygen mass flow rate. The mixture ratio $E = \dot{m}_{LOx}/\dot{m}_{H_2}$ is 8.8 (at the intermediate pressure of 3.6 MPa) and 1.86 under steady operation at 6.3 MPa. The value of the gas to liquid momentum flux ratio J is equal to 0.7 at $p = 3.6$ Mpa and 8.5 at high pressure. This quantity is not perfectly constant at each pressure stage because it depends on a ratio of velocities square. The two pressure levels of operation are examined successively.

Point of operation	$\dot{m}_{LOx}$ (g/s)	$\dot{m}_{H_2}$ (g/s)	v (ms^{-1})		π_r	
			O_2	H_2	O_2	H_2
IP	65	7.5	3	46	0.72	2.8
HP	92	50	4	180	1.26	5

Table 1: Selected operating conditions. IP corresponds to the intermediate pressure stage while HP pertains to high pressure conditions. Data are averaged on each pressure stage.

3.1. Intermediate pressure conditions

In the first pressure stage ($p \sim 3.6$ MPa) the value of the momentum flux ratio is low and one expects in this case that the flame will not be well established. The chamber pressure is below the critical value of oxygen ($p_c = 5.04$ MPa) and the injected liquid stream undergoes a classical cascade of processes associated with break-up, atomization vaporization and combustion. Typical distributions of OH fluorescence intensity are displayed in Fig. 2. While the pressure is already quite high ($p = 3.6$ MPa), the signal to noise ratio is sufficient (SNR$\simeq$ 20 dB), and well defined PLIF images are obtained. Flame structures are well detected in the lower half of the domain. As the optical depth of the medium decreases with pressure, the laser beam is partially attenuated

by OH absorption before being totally distorted by the high density liquid oxygen jet explaining the absence of fluorescence signals in the upper part of the chamber. The light scattered by the liquid jet is not detected by the ICCD camera indicating that the filtering scheme adopted in these experiments is adequate and that fluorescence from OH constitutes the major part of the light detected by the camera. In the injector nearfield the flame expands sharply and some local extinctions can be identified. The flame is not well anchored to the oxygen injector lip and not really established in the combustion chamber. It does not wrap around the liquid jet as observed in [3] or [6] under more standard injection conditions. Instantaneous images of OH^* emission (Fig. 3) taken with the wide field camera also feature a poorly established flame which does not spread smoothly in the downstream direction and is not well balanced in the upper and lower sides of the injector. The OH* emission distribution forms a compact pocket in the lower part of the combustor.

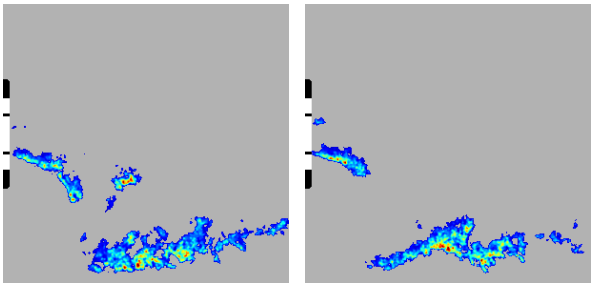

Fig. 2: OH PLIF images in the injector nearfield recorded during the intermediate pressure stage, $p = 3.8\,\text{MPa}$, $J = 1.5$. The image ends at 8 d_{LOx} from the injection plane.

The low pressure point of operation typifies transient phases where the injected propellants are not well equilibrated and feature an off-range momentum flux ratio. One expects a degraded atomization of the liquid jet inducing local extinctions with a possible flame blow-off. From cold flow experiments and theoretical considerations [7, 8], it was suggested that the momentum flux ratio J was the most influential parameter in determining the rupture of the central fluid in a coaxial jet at least under subcritical conditions. Low pressure range experiments ($p = 1\,\text{MPa}$) carried out by [9] have confirmed that J controls flame spread. For a given couple of propellants, it was shown that a critical value of J existed above which the quality of atomization ensured a well expanded flame. In that range, the oxygen stream behaves like a liquid jet which is broken into ligaments which are subsequently atomized by aerodynamic shear stresses induced by the high speed hydrogen flow. When J is too low, the quality of the break-up process is poor because the gaseous stream impulse is too low to correctly atomize the liquid oxygen jet and this in turn gives rise to an irregular and unstable flame as confirmed in this experiment.

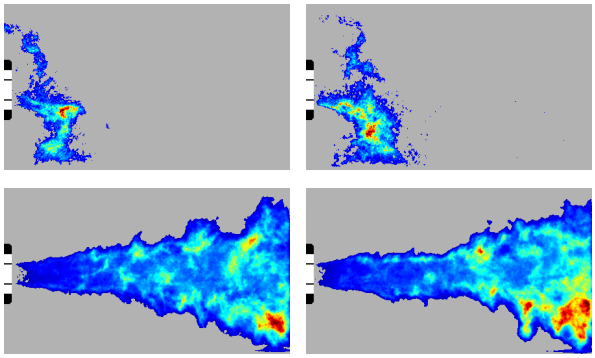

Fig. 3: Top : Typical OH^* emission images recorded during the intermediate pressure stage, $p = 3.8\,\text{MPa}$, $J = 1.5$. The flame is not well established and highly unstable. Bottom : Typical OH^* emission images recorded during the high pressure stage, $p = 6.3\,\text{MPa}$, $J = 9$. Flame spreading is normal.

3.2. High pressure conditions

In the second part of the test ($p \sim 6.3\,\text{MPa}$) the critical pressure of oxygen is exceeded. The liquid jet undergoes a transcritical change of state. Its dynamics notably differs from that prevailing in the low pressure range. The well defined liquid-gas interface is replaced by a thin mixing region established between the dense, low temperature high density transcritical oxygen jet and low density supercritical gaseous oxygen. Mass transfer across this layer controls the process and determines the rate at which chemical reaction may take place in the gaseous phase. Typical distributions of OH fluorescence intensity are displayed in Fig. 4. At the operating pressure of $6.3\,\text{MPa}$ the signal to noise ratio (SNR$\simeq$ 14 dB) is still acceptable but somewhat lower than that found at the intermediate pressure $p = 3.8\,\text{MPa}$. An examination of the instantaneous images, indicates that the flame spreads in a standard way. The initially thin flame layer rapidly features wrinkles and pockets. The flame is close to the oxygen injector lip but the flame edge is established at

various locations on the downstream side of this unit (see below). In the injector nearfield, the flame structure can be divided in two regions. In the first the reaction zone moves towards the oxygen jet. In the second region the flame expands outwards in a more progressive manner. The OH^* emission images corresponding to high pressure operation (bottom part of Fig. 3) also show a well developed flame attached to the injector and spreading in the downstream direction.

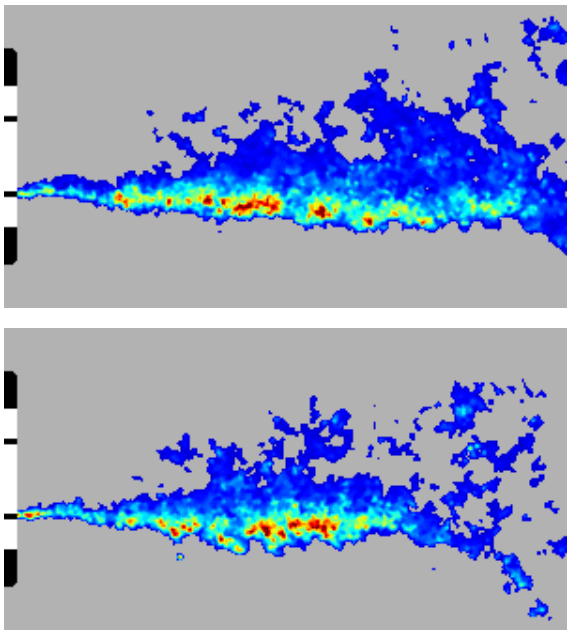

Fig. 4: OH PLIF images in the injector nearfield recorded during the high pressure stage, $p = 6.3\,\mathrm{MPa}$, $J = 9$. The cryogenic flame is thin, well established and anchored to the oxygen injector lip. At a distance from the injector the flame sheet is wrinkled by turbulent fluctuations.

Transcritical fluid behaves like a gas but with a highly non uniform density distribution. In the central core where the temperature is below critical, the density is very high and combustion cannot proceed in that region. In the outer layer of the core region where the temperature has increased and is above the critical value, the density is low and some reactions may take place indicating that fluorescence signals may originate from these regions. Under these conditions, the structure of the flame is controlled by the rate of mass transfer from the liquid oxygen stream rather than by the momentum flux ratio J. The oxygen transfer process is mainly governed by turbulence and mixing [2, 10, 11]. This in turn is determined by the velocity difference between the two streams. The flame is formed behind a step between non premixed hydrogen and gaseous oxygen. Hydrogen is injected at high speed contrary to liquid oxygen and the mixture ratio E is low compared to the stoichiometric value. Combustion occurs at near stoichiometric conditions and the flame develops between the two propellants in the wake of the LOx-post lip. Under these conditions, the isostoichiometric surface around which the flame develops forms a shell in the low oxygen density region surrounding the dense oxygen jet. This surface is initially close to the dense jet because gaseous oxygen is not yet available. The flame is wrapped around the liquid core and heat is transferred to the dense oxygen to generate gaseous oxygen. Further downstream, the reaction zone spreads outwards as mass transfer between dense and light regions is enhanced.

4. Flame stabilization in the nearfield

The OH fluorescence images may now be used to examine the flame stabilization region. In the specific case of coaxial injection of cryogenic propellants, previous studies have indicated that the flame edge is close to the injector lip and that it is therefore in the near vicinity of the high speed hydrogen stream. It is important to understand how this is achieved and determine conditions required to obtain a steady flame anchoring. This is essential since a lack of stabilization may lead to the emergence of combustion instabilities or flame blow-off.

Previous experiments indicate that the flame edge is close to the LOx injector lip and that it is formed by slow moving oxygen and hydrogen which meet and react just behind the lip. A detailed analysis of the flow in the lip neighborhood indicates that the flame is anchored when its thickness is smaller than the transverse dimension of the wake established by the injector lip [12]. This wake has a typical size which is of the order of the lip thickness and it is in fact possible to devise a stabilization criterion which compares the lip size h_s to the flame thickness δ_f and define the characteristic ratio $\Psi h_s/\delta_f$. Calculations indicate that the flame is anchored when $\Psi > 1$ and becomes unstable and sensitive to the high speed stream when $\Psi < 1$.

Laser induced fluorescence may be used to see if the thickness satisfies the previous stability condi-

tion. It is also worth comparing the experimental OH distribution to flame structures determined numerically notably by [13, 14] using LES tools for transcritical combustion. It is shown in these references that the flame is stabilized on the oxygen injector lip and develops in the near vicinity of the oxygen stream. The flame edge is stuck to the lip and the reaction front develops near the oxygen boundary and becomes highly wrinkled further downstream. Space-time resolved OH PLIF images may provide some essential information on the structure and spatial fluctuations of the flame edge.

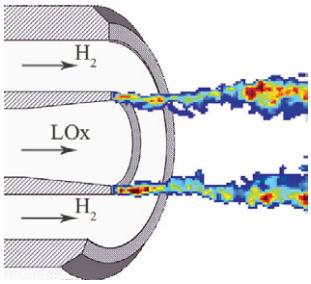

Fig. 5: Instantaneous flame structure in the coaxial injector near field. Close-up corresponds to the first two LOx-post diameters. The figure is based on two different instantaneous PLIF images.

Figure 5 shows a close up view of the first two LOx tube diameters downstream the injection plane. This representation, synthesized by making use of two instantaneous PLIF images shows how the flame spreads with regard to the injector. The reactive layer begins at the lip and moves inwards following a contracted high density oxygen core. The reactive layer thickness later increases by wrinkling as the mixing layer between hydrogen and gaseous oxygen grows. After about one diameter d_{LOx} the flame spreads outwards as low density oxygen is accumulated around the high density core. It is now interesting to take a closer look at the flame edge established near the lip by first augmenting the resolution [1]. for more details). The OH layer appears at various locations with respect to the injector lip. The flame edge is moving around and the direction of the OH distribution also changes from one view to the next as shown in Fig. 6. This indicates that some unsteadiness affects the flame anchor point. It also appears that the OH layer thickness is of the order of the lip thickness indicating that the flame is sensitive to the high speed hydrogen stream. It is known from a previous analysis [12] that when this occurs, stabilization is imperfect. Flame blow-off may take place under these circumstances. This does not happen here because the flame is probably close to the injector lip at some other circumferential locations.

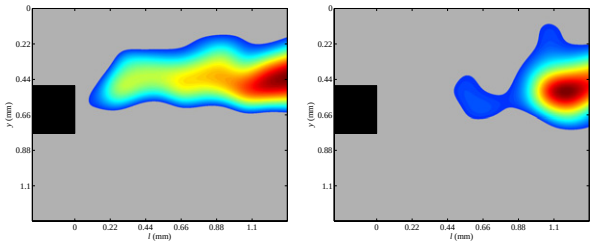

Fig. 6: OH-PLIF images of the flame holding region. Liquid oxygen and gaseous hydrogen are injected above and below the step respectively. The OH distribution in the flame edge is shown on the standard color scale.

5. Conclusion

It is shown in this article that good quality laser induced fluorescence images may be obtained under high pressure conditions ($p \sim 6.3\,\mathrm{MPa}$). The study focuses on fluorescence of OH in gaseous hydrogen/liquid oxygen cryogenic flames. Fluorescence images of the injector nearfield provide instantaneous distributions of OH radicals. These data confirm that the flame is initiated in the near vicinity of the liquid oxygen injector lip. The thickness of the OH layer grows as the mixing layer expands downstream and features wrinkles and inhomogeneities corresponding to local accumulation and changes of the reaction rate as a function of the strain rates acting on the local flame elements. Numerical close-up views of the oxygen injector lip region show that the flame edge is sensitive to the outer high velocity free stream. Some unsteadiness affects the flame anchor point indicating that the lip size is not large enough to ensure a perfect stabilization.

Acknowledgments

This work was supported by CNES, Snecma, CNRS and Institut Universitaire de France. The help of the Mascotte team of Onera under the leadership of Lucien Vingert is gratefully acknowledged.

References

[1] G. Singla, P. Scouflaire, J. Rolon, S. Candel, *Combustion and Flame* (2005) Submitted.
[2] G. Singla, P. Scouflaire, J. Rolon, S. Candel, *Proceedings of the Combustion Institute* 30 (2005) 2921–2928.

[3] M. Juniper, A. Tripathi, P. Scouflaire, C. Rolon, S. Candel, *Proceedings of the Combustion Institute* 28 (2000) 1103–1109.
[4] B. Atakan, J. Heinze, U. Meier, *Applied Physics B: Lasers and Optics* 64 (1997) 585–591.
[5] M. Juniper, Structure and stabilization of cryogenic spray flames, Ph.D. thesis, Ecole Centrale Paris (2001).
[6] G. Herding, R. Snyder, C. Rolon, S. Candel, *Journal of Propulsion and Power* 14 (1998) 146–151.
[7] J. Lasheras, E. Villermaux, E. Hopfinger, *Journal of Fluid Mechanics* 357 (1998) 351–379.
[8] H. Rehab, E. Villermaux, E. Hopfinger, *Journal of Fluid Mechanics* 345 (1997) 357–381.
[9] R. Snyder, G. Herding, J. Rolon, S. Candel, *Combustion Science and Technology* 124 (1997) 331–370.
[10] J. Bellan, *Progress in Energy and Combustion Science* 26 (2000) 329–366.
[11] V. Yang, *Proceedings of the Combustion Institute* 28 (2000) 925–942.
[12] M. Juniper, S. Candel, *Journal of Propulsion and Power* 10 (2003) 332–441.
[13] J. Oefelein, V. Yang, *Journal of Propulsion and Power* 14 (1998) 843–857.
[14] J. Oefelein, *Proceedings of the Combustion Institute* 30 (2005) 2929–2937.